Fluidification of entangled polymers by loop extrusion

Filippo Conforto [1], Yair Gutierrez Fosado [1], and Davide Michieletto [1,2,*]

[1] *School of Physics and Astronomy, University of Edinburgh, Peter Guthrie Tait Road, Edinburgh, EH9 3FD, United Kingdom*

[2] *MRC Human Genetics Unit, Institute of Genetics and Cancer, University of Edinburgh, Edinburgh EH4 2XU, United Kingdom*

(Received 31 January 2024; accepted 25 July 2024; published 12 August 2024)

Loop extrusion is one of the main processes shaping chromosome organization across the cell cycle, yet its role in regulating deoxyribonucleic acid (DNA) entanglement and nucleoplasm viscoelasticity remains overlooked. We simulate entangled solutions of linear polymers under the action of generic loop extruding factors (LEFs) with a model that fully accounts for topological constraints and LEF-DNA uncrossability. We discover that extrusion drives the formation of bottlebrushlike structures which significantly lower the entanglement and effective viscosity of the system through an active fluidification mechanism. Interestingly, this fluidification displays an optimum at one LEF every 300–3000 base pairs. In marked contrast with entangled linear chains, the viscosity of extruded chains scales linearly with polymer length, yielding up to 1000-fold fluidification in our system. Our results illuminate how intrachain loop extrusion contributes to actively modulate genome entanglement and viscoelasticity *in vivo*.

DOI: 10.1103/PhysRevResearch.6.033160

I. INTRODUCTION

How chromosomes are packaged within the cell while remaining accessible to transcription, replication, and segregation remains one of the most fascinating unsolved problems in physics and biology. Chromosome conformation capture and related techniques [1,2] have revealed that chromosomes are folded into so-called territories, compartments, and topologically associated domains [3–6]. Among the most important processes dictating chromosome folding in both interphase and mitosis is loop extrusion, performed by so-called loop extruding factors (LEFs), such as cohesin, condensin, and SMC5/6 [7–13,13–17]. Most of the current experimental techniques study either static snapshots of LEF-mediated chromosome conformation *in vivo* [16] or dynamic LEF-mediated looping process on tethered single deoxyribonucleic acid (DNA) molecules *in vitro* [12]; and only very recently was it possible to track the behavior of individual chromosome loci under the effect of loop extrusion [18]. Due to this, we still lack a quantitative understanding of how LEFs modulate chromosome dynamics and entanglements in the dense, crowded, and entangled environment of the cell nucleus. To tackle this question, we perform large-scale molecular dynamics simulations of entangled fluids of linear polymers under the action of LEFs. Specifically, we study how loop extrusion affects polymer conformation, dynamics, and viscoelasticity during mitosislike and interphaselike stages of loop extrusion, by modulating their number, processivity, and turnover.

First, we find that (exclusively intrachain) loop extrusion induces a transition from linear polymers to bottlebrushlike structures, characterized by large grafting density and side-chain length controlled by the number and processivity of the LEFs, in line with previous works in dilute conditions [9,19–21]. The formation of such structures reduces the entanglement between chains due to steric interactions between the loops and entropy maximization—an effect dubbed *entropic repulsion* [22,23], in turn leading to the fluidification of the system. Second, we discover that, while as few as ∼2–100 LEFs per 30 kbp of chromatin are enough to induce a significant reduction in entanglement, a larger number of LEFs is not as effective due to the reduced repulsion of side chains and stiffening of the chain backbone. We find that extrusion enables an active fluidification process that can reduce the viscosity of long extruded polymers by three orders of magnitude with respect their nonextruded (NE) equivalent. Finally, we show that even LEFs with binding/unbinding kinetics can drive active fluidification in entangled fluids. Our work is different from other simulations on LEF-mediated disentanglement of polymers [19,21,24–27], as we focus on the bulk viscoelastic behavior of dense polymer solutions rather than structure of loop-extruded polymers in dilute conditions. We not only numerically confirm recent theoretical arguments suggesting that loop extrusion yields an entanglement dilution [21,26], but we also quantify the degree of disentanglement in dense solutions through primitive path analysis (PPA) and, more importantly, its impact on the rheology of the system. More specifically, our results suggest that, by varying the number and processivity of LEFs, the cell may be able to finely regulate entanglements between chromosomes and, in turn, the nucleoplasm effective viscoelasticity, which could be tested in large-scale imaging and spectroscopy experiments [28–30].

*Contact author: davide.michieletto@ed.ac.uk

Published by the American Physical Society under the terms of the Creative Commons Attribution 4.0 International license. Further distribution of this work must maintain attribution to the author(s) and the published article's title, journal citation, and DOI.

II. METHODS

A. Simulation details

We model entangled DNA as semiflexible Kremer-Grest linear polymers [31] with $N = 250$, 500, 1000, and 1500 (unless otherwise stated) beads of size σ. The beads interact with each other via a truncated and shifted Lennard-Jones potential:

$$U_{\mathrm{LJ}}(r) = \begin{cases} 4\epsilon\left[\left(\frac{\sigma}{r}\right)^{12} - \left(\frac{\sigma}{r}\right)^{6} + \frac{1}{4}\right], & r \leqslant r_c, \\ 0, & r > r_c, \end{cases} \quad (1)$$

where r denotes the separation between the beads, and the cutoff $r_c = 2^{1/6}\sigma$ is chosen so that only the repulsive part of the potential is used. Nearest-neighbor monomers along the contour of the chains are connected by finitely extensible nonlinear elastic (FENE) springs as

$$U_{\mathrm{FENE+LJ}}(r) = \begin{cases} -0.5kR_0^2 \ln\left[1 - \left(\frac{r}{R_0}\right)^2\right] + U_{\mathrm{LJ}}, & r \leqslant R_0, \\ \infty, & r > R_0, \end{cases} \quad (2)$$

where $k = 30\epsilon/\sigma^2$ is the spring constant and $R_0 = 1.5\sigma$ is the maximum extension of the elastic FENE bond. This choice of potentials and parameters is essential to preclude thermally driven strand crossings and therefore ensures that the global topology is preserved at all times [31,32]. Finally, we add bending rigidity via a Kratky-Porod potential $U_{\mathrm{bend}}(\theta) = k_\theta(1 - \cos\theta)$, where θ is the angle formed between consecutive bonds, and $k_\theta = 5k_BT$ is the bending constant, thus yielding a persistence length $l_p = 5\sigma$, corresponding to 50 nm in our grained model. We chose these parameters to facilitate the comparison with *in vitro* experiments, i.e., to model the behavior of naked DNA at physiological salt condition resulting in a screening length of 10 nm and a persistence length of 50 nm. The motion of each bead is then evolved via the Langevin equation:

$$m\frac{dv_i}{dt} = -\gamma v_i - \nabla U + \sqrt{2k_BT\gamma_i}\eta, \quad (3)$$

along each Cartesian component. Here, γ is the friction coefficient, m the mass of the bead, U the sum of the potentials acting on bead i, and $\sqrt{2k_BT\gamma}\eta$ a noise term that obeys the fluctuation-dissipation theorem, thus respecting the formula:

$$\left\langle \eta_i^\alpha(t)\eta_j^\beta(s)\right\rangle = \delta(t-s)\delta_{ij}\delta_{\alpha\beta}, \quad (4)$$

along each Cartesian component (Greek letters). The numerical evolution of the Langevin equation is done with a velocity-Verlet scheme with $dt = 0.01\tau_{\mathrm{LJ}}$, with $\tau_{\mathrm{LJ}} = \tau_{\mathrm{Br}} = \sigma\sqrt{m/\epsilon}$ in LAMMPS [33].

Four different systems are considered in this paper: the first one consists of a solution of 50 linear polymers having size 1000 in a cubic box of side length 80.6 [Fig. 1(g)], achieving a monomer density of ∼10%, equivalent to a volume fraction of $\phi = 0.05$. We maintained the same monomer density on systems containing polymers 250σ, 500σ, and 1500σ long by reshaping the box size, respectively, to 51σ, 64σ, and 92σ.

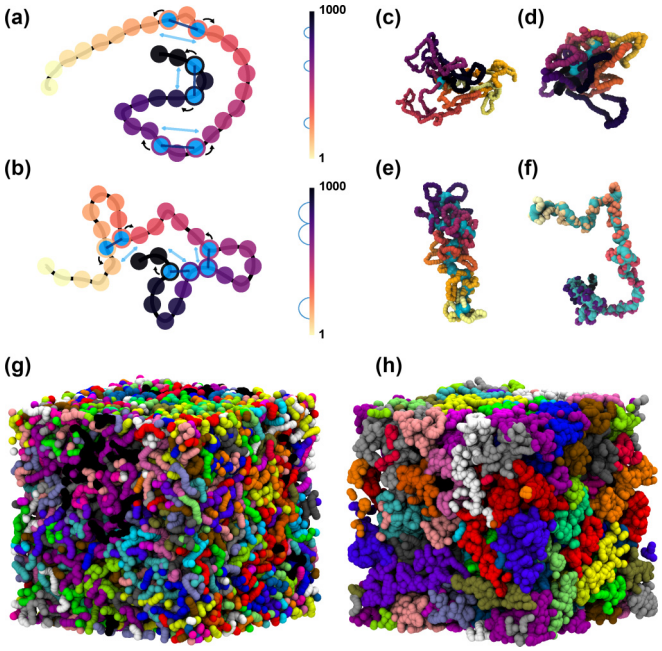

FIG. 1. (a) and (b) Sketch of our loop extruding factor (LEF) algorithm on a coarse-grained polymer. Each LEF stops when it meets another LEF along the chain. (c)–(f) Snapshots of fully extruded polymers with (e) $n_{\mathrm{LEF}} = 2$, (f) $n_{\mathrm{LEF}} = 10$, (g) $n_{\mathrm{LEF}} = 100$, and (h) $n_{\mathrm{LEF}} = 200$. Cyan beads represent LEFs. (g) Snapshot of the system consisting of $M = 50$ linear polymers of length $N = 1000$ in a box of size $L = 80.6\sigma$ and periodic boundary conditions. (h) Snapshot of the system after intrachain extrusion with an average of 100 LEFs per polymer. In (a)–(f), the color gradient represents the bead index, while in (g)–(h), the colors represent different polymers. See Supplemental Video for more information [34].

B. Modeling loop extrusion

Our loop extrusion model was inspired by previous works [9,19]. In these models, loops are formed by temporary bonds joining two beads, thus generating closed rings emerging from the polymer backbone. Loop extrusion is then achieved by shifting each bond to the adjacent beads on both sides of the bond, as shown in Fig. 1(a). Bond shifting introduces energy into the system, mirroring the adenosine triphosphate (ATP) hydrolysis cycle in structural maintenance of chromosomes (SMC) proteins, and it breaks detailed balance. However, most models in the literature allow nonphysical extrusion, as the bond shift is performed irrespectively of the distance between the newly selected beads. This is often possible thanks to the use of unbounded harmonic bonds, allowing large distances between the loop ends and possibly leading third segments to pass through the bonded segments. We argue that this nonphysical feature should be avoided, as we expect SMC complexes to block possible strand passages between their ends, and that extrusion should consider the geometry and topology of the DNA molecule [25]. Therefore, we developed a customized version of a LAMMPS fix module publicly available online [35], and used version v30_06_23 for this paper. Specifically, we attempt extrusion steps with a fixed frequency f_{att}, chosen at the beginning of the simulation. On top of that, we define a success probability f_{prob} for the extrusion step that

adds up to the geometry check. Then the distance between the ends of new LEFs is computed, and the step is accepted only if its value is smaller than a fixed cutoff $r < 1.2\sigma$. Each LEF attempts an effective step with frequency $f_{\text{eff}} = f_{\text{att}} f_{\text{prob}}$, in turn slowing down the actual extrusion speed along the polymer because of conformational entropy. All the simulations in this paper are performed with $f_{\text{eff}} = 1 \times 10^{-3}\,\tau_{\text{Br}}^{-1}$. If during the extrusion process two LEFs meet on one end, extrusion proceeds only on one side, as displayed in Fig. 1(b). Consequently, extrusion runs for each LEF until one of its ends neighbors the end of another LEF or reaches the polymer ends.

In practice, we implement loop extrusion by initializing a given number of LEFs by choosing random triplets of beads belonging to the polymers in solution. This provides each polymer with a total number of bound LEFs on average equal to n_{LEF}. However, to neglect the presence of unextruded polymers, we deploy at least one LEF on every polymer. To prevent integration errors related to the bond length, we initially model LEFs with a harmonic bond, with potential:

$$U_{\text{harm}}(r) = A(r - R_0)^2, \tag{5}$$

where $A = 100$ and $R_0 = 1.1\sigma$. After the first step, such a bond is replaced by a FENE bond with $k = 10$ and $R_0 = 1.7\sigma$ [see Eq. (2)]. We choose a larger maximum extension for the elastic FENE bond and a softer spring constant to avoid bond breaking caused by sudden movement of the bonds during extrusion. In contrast with recent works [36,37], here, we consider purely intrachain loop extrusion with no bridging interaction between LEFs [Figs. 1(a) and 1(b)].

C. Mean squared displacement and radius of gyration

The mean squared displacement (MSD) at time τ measures the motion of a polymer segment with respect to the initial position over a time τ. It is computed as

$$\text{MSD}(\tau) = \frac{1}{N}\frac{1}{T-\tau}\sum_{t=0}^{T-\tau}\sum_{i=1}^{N}[x^i(t+\tau) - x^i(t)]^2. \tag{6}$$

For entangled linear polymers, we expect the MSD of the center of mass (COM) of the polymer to be $\text{MSD}(\tau) \sim \tau^{1/2}$ for short time scales and $\text{MSD}(\tau) \sim \tau$ on long time scales [38]. The squared radius of gyration of a polymer is computed as

$$R_g^2 = \frac{1}{N}\sum_{k=1}^{N}[r_k - r_{\text{mean}}]^2, \tag{7}$$

where r_{mean} defines the COM of the polymer.

D. PPA

PPA is a method to compute the entanglement length in a solution of polymers [39]. We apply PPA to 10 different restart configurations for each simulated system, sampled at times separated by $2 \times 10^5\,\tau_{\text{Br}}$ to obtain uncorrelated states. The protocol used for PPA involves disabling intrachain interactions while preserving interchain interactions and keeping the ends of polymers fixed in space. To measure the entanglement between the backbones, we remove the beads belonging to the loops, whereas in regular PPA, the bonds forming loops are deleted. The temperature of the Langevin thermostat is set at $T = 0.001\epsilon/k_B$, and the simulation is run for 5×10^5 time steps. We perform five of these simulations for each sampled configuration. The systems thus obtained display a collapse of the polymers over the key entanglement points, from which the entanglement length can be computed as

$$L_e = \frac{D_{e2e}^2}{N_{\text{beads}}\overline{D_{\text{bond}}}^2}, \tag{8}$$

where D_{e2e} represents the end-to-end distance of the polymer and $\overline{D}_{\text{bond}}$ the average bond length in the polymer.

E. Green-Kubo calculation

The stress-relaxation modulus $G(t)$ is calculated as

$$G(t) = \frac{V}{3k_bT}\sum_{\alpha\neq\beta}\bar{P}_{\alpha\beta}(0)\bar{P}_{\alpha\beta}(t), \tag{9}$$

where $\bar{P}_{\alpha\beta} = \bar{P}_{xy}$ and $\bar{P}_{xz}$ and $\bar{P}_{yz}$ represents the off-diagonal components of the stress tensor. Specifically, we get those components as

$$\bar{P}_{\alpha\beta}(t) = \frac{1}{t_{\text{avg}}}\sum_{\Delta t=-\frac{t_{\text{avg}}}{2}+1}^{t_{\text{avg}}} P_{\alpha\beta}(t+\Delta t), \tag{10}$$

$$P_{\alpha\beta}(t) = \frac{1}{V}\left(\sum_{k=1}^{NM} m_k v_k^\alpha v_k^\beta + \frac{1}{2}\sum_{k=1}^{NM}\sum_{l=1}^{NM} F_{kl}^\alpha r_{kl}^\beta\right), \tag{11}$$

where N is the number of beads per polymer, M the number of polymers, V the box volume, m_k the mass of the kth bead, v_k the speed of the kth bead, F_{kl} the force between the kth and lth beads, and r_{kl} their distance. Here, $P_{\alpha\beta}$ is then averaged over a time t_{avg} [40]. The autocorrelation was computed using the multiple-τ correlator method described in Ref. [41] and implemented in LAMMPS with the fix ave/correlate/long command. This method makes sure that the systematic error of the multiple-τ correlator is always below the level of the statistical error of a typical simulation (see LAMMPS documentation). The viscosity η of the system is then obtained by integrating $G(t)$ as

$$\eta = \int_0^{t\to\infty} G(t)dt.$$

Given that our simulations are run for a finite time, the computed viscosity represents a lower bound for the true value. Such a value is then obtained in simulation units $\frac{k_BT\tau_{\text{Br}}}{\sigma^3}$ where $\tau_{\text{Br}} = \frac{3\pi\eta_s\sigma^3}{k_BT} = 2.6\,\mu\text{s}$.

To account for the noisy values appearing on large time-step values, we model the behavior of $G(t)$ as a stretched exponential at large times. Specifically, we define $G(t) \approx a\exp[(-\frac{t}{\tau})^b]$, and we fit a, τ, and b to approximate the exponential decay, starting at an arbitrarily found point, denoted as t_e. The viscosity is then obtained by numerical integration up to t_e, while the stretched exponential contribution is obtained by computing $\int_{t_e}^{\infty} a\exp[(-\frac{t}{\tau})^b] = \frac{a\tau}{b}\Gamma[\frac{1}{b}, (\frac{t_e}{\tau})^b]$, where $\Gamma(a,z)$ is the upper generalized gamma

function. The sum between these two terms returns the viscosity estimate.

The Green-Kubo (GK) measurements are done in equilibrium in the fully extruded (FE) cases. On the other hand, during transient extrusion, polymers are out of equilibrium because LEFs are imposing nonthermal forces on them. Despite this, GK relations work in nonequilibrium steady-state systems in specific conditions [42]. To demonstrate that the loop extrusion *per se* does not affect our GK calculation, we selected four different time steps separated by $2 \times 10^6 \tau_{\mathrm{Br}}$ (significantly larger than the autocorrelation time of the squared radius of gyration in steady state, estimated to be $\sim 5 \times 10^5 \tau_{\mathrm{Br}}$) of a system with 10 LEFs per polymer and $\kappa_{\mathrm{off}} = 10^{-8} \tau_{\mathrm{Br}}$. We then blocked the extrusion process for each of these initial conditions, waited for $5 \times 10^6 \tau_{\mathrm{Br}}$, sufficient to allow polymer equilibration, and measured $G(t)$. We find that the GK stress-relaxation curve is independent of the specific state of the system once steady state is reached and is identical to the one computed during the extrusion process (i.e., when it is not stopped). This means that the loop extrusion does not affect the viscoelasticity of the sample *per se* and that the most important contribution to the rheology is the change in polymer conformation. We argue that this is due to the extrusion regime we work in, as the extruded loops relax on time scales shorter than the time between LEF steps [26]. In turn, this leads to a virtually relaxed state in which polymer conformations are the main contribution to the viscoelastic properties. In other regimes, a correction to $G(t)$ would be needed to account for the energy-consuming nonequilibrium processes.

F. Processivity

We define a transient extrusion regime in which LEFs load/unload dynamically at rates κ_{on} and κ_{off}, respectively. In this regime, we define processivity as $\lambda = \frac{v_{\mathrm{LEF}}}{k_{\mathrm{off}}}$, but in many of our simulations, the true speed of LEFs is hardly measurable. In FE systems, since k_{off} is zero, this value is assumed to be on average equal to the polymer length divided by the average number of LEFs per polymer. Instead, when $k_{\mathrm{off}} > 0$, we decided to compute the single LEF processivity and consider the average its distribution. Such a distribution is found to be corresponding to a Poissonian process, in agreement with our probability-dependent LEF removal.

G. Modeling SMCs

SMC extrusion speed is of the order of $1\,\mathrm{kbp\,s^{-1}}$ [12]. In our simulation, the effective maximum speed is obtained by accepting all the moves with frequency f_{eff}, which for symmetric steps gives $v_{\mathrm{max}} = 2\sigma f_{\mathrm{eff}} = 2 \times 10^{-3} \sigma \tau_{\mathrm{Br}}^{-1}$ for $f_{\mathrm{eff}} = 10^{-3} \tau_{\mathrm{Br}}^{-1}$. Since each bead coarse grains $\sim 30\,\mathrm{bp}$ of naked DNA, we have $v_{\mathrm{max}} \sim 26\,\mathrm{kbp\,s^{-1}}$. However, this maximum speed is hardly reached during simulations because of the cutoff value. In a system that allows transient binding of LEFs, we can get an estimate of the effective extrusion speed by multiplying the average processivity by the unbinding rate k_{off}. For values of $\frac{\lambda}{\langle d \rangle} \sim 1$, this speed is found to be on the order of $10^{-5} \sigma \tau_{\mathrm{Br}}^{-1}$.

III. RESULTS

A. Loop extrusion drives compaction and dilution of entanglements

As explained in the Methods, we perform loop extrusion on dense and entangled polymer solutions. First, we qualitatively observe that the extrusion induces a geometrical deformation of the polymers into bottlebrushlike structures, as previously noticed [19–21,26] [Figs. 1(c)–1(f)]. Interestingly, this is accompanied by the onset of compartmentalization and territories, with the polymers becoming less intermingled [24] [see Figs. 1(g) and 1(h)]. The radius of gyration R_g^2 displays a sharp reduction during the extrusion process [Fig. 2(a)]. We then proceed to characterize the solution in equilibrium, when the squared radius of gyration plateaus and loop extrusion has stopped as LEFs are adjacent along the polymers. To make sure that our system is in equilibrium, we perform measurements once the MSD has reached $\langle R_g^2 \rangle$ at steady state. At a large value of time, the steady-state value $\langle R_g^2 \rangle$ displays nonmonotonic behavior, which we understand as a direct consequence of the bottlebrush structure [e.g., see snapshots in Figs. 1(c)–1(f)]: A larger number of LEFs effectively induces a larger grafting density and longer backbones, which contribute to an increase of R_g^2. The observed stiffening is in agreement with both theory [22] and experiments [43] of synthetic bottlebrush polymers, as backbone stiffening is expected at larger grafting density due to increased entropic and stering interactions between the side chains. Additionally, from the snapshots of single chains in Fig. 1, one can appreciate the change in polymer conformation as a function of the number of bound LEFs: from that of a dense comb polymer (a small number of long side chains) to dense bottlebrush (a large number of short side chains) [23,43].

To understand how the conformational transition affects entanglements, we perform PPA to the extruded solutions [39,44] [Figs. 2(b) and 2(c)]. According to Ref. [44], we can estimate the entanglement length N_e as

$$N_e = l_K \left[\left(c_\xi \rho_K l_K^3 \right)^{-2/5} + \left(c_\xi \rho_K l_K^3 \right)^{-2} \right], \tag{12}$$

where $c_\xi = 0.06$, $l_K = 2l_p$ is the Kuhn length, and $\rho_K = NM/(l_K L^3)$ is the number density of Kuhn segments. We find that NE solutions have an average entanglement length $N_e = 96 \pm 65\sigma$, somewhat larger than the theoretically expected value $N_e = 43\sigma$ yet within error.

Like what was done in Ref. [45] for solutions of bottlebrush polymers, we first performed PPA on the polymer backbones by removing the side loops [Fig. 2(d)]. All the extruded solutions display significant disentanglement compared with the NE control system ($n_{\mathrm{LEF}} = 0$). However, we expect side loops not to be entangled when the polymers display many short loops, so that they cannot thread each other [46,47]. To quantify the entanglement between side loops, we performed PPA on the whole polymers. We note that, in this case, the overall chains are non-Gaussian. Still, the entanglement length displays an interesting behavior: At small $n_{\mathrm{LEF}} = 2$, the system appears more entangled than the NE control case [Fig. 2(e)], and that N_e grows larger only when more LEFs are bound to the polymers. By visually inspecting the simulations, we found that the reason behind this behavior is the presence of deadlocks [see inset Fig. 2(e)]. It is

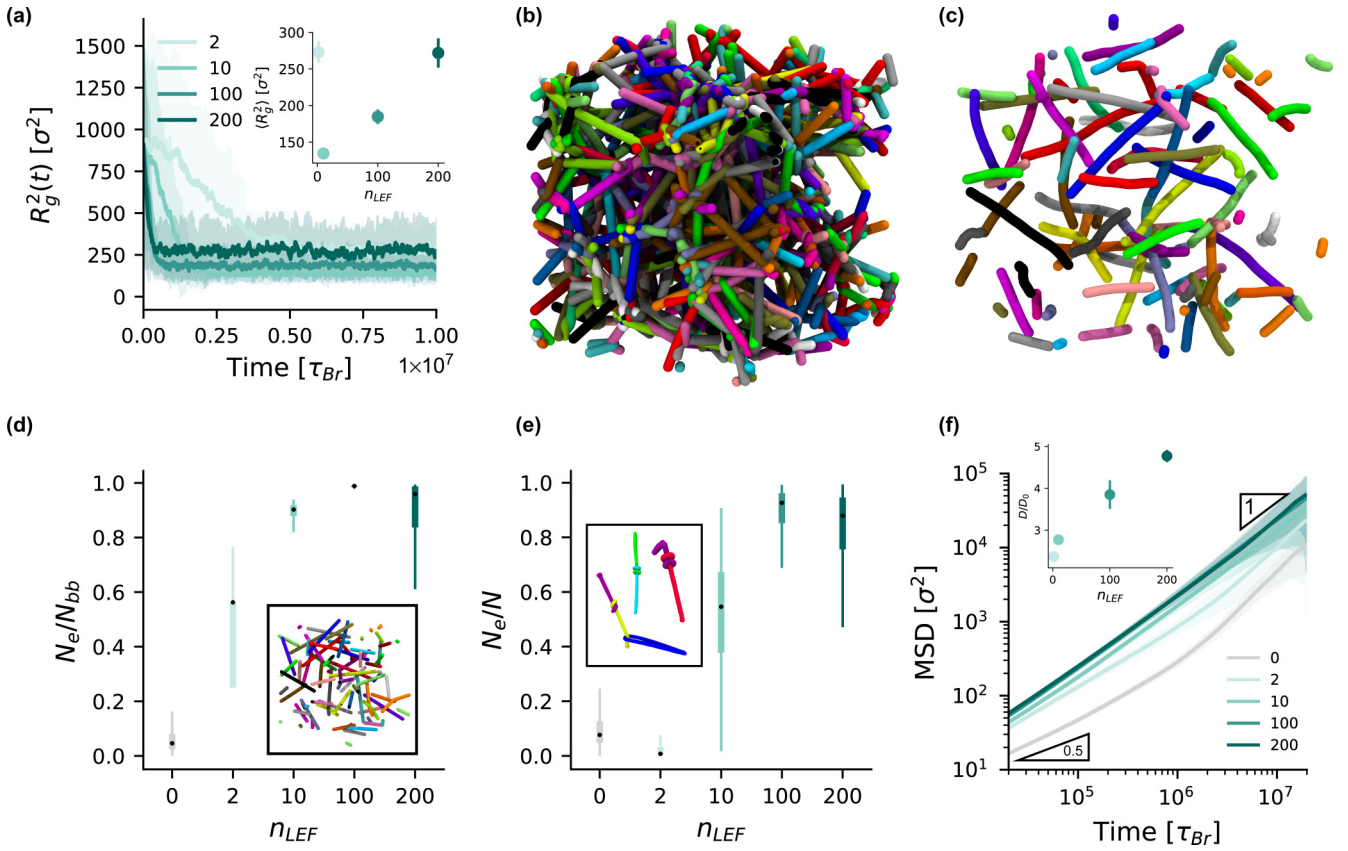

FIG. 2. Equilibrium viscoelastic properties of monodisperse solutions with $N = 1000$ for different values of n_{LEF}. (a) Average radius of gyration of polymers during extrusion and after equilibration. The faded area represents the width of the area covered by the distribution within the standard deviation. Inset shows the equilibrium value against n_{LEF}. Snapshots of simulated systems after temperature quenching for (b) a nonextruded solution and (c) an extruded solution. (d) Box plot representing the distribution of backbones entanglement lengths over the polymer length (number of extruders per polymer) obtained through primitive path analysis (PPA) [39] on a set of 5 uncorrelated replicas over 10 different time steps. The inset shows the final primite paths for $n_{\mathrm{LEF}} = 2$. (e) Box plot representing the distribution of entanglement lengths over polymer length obtained through PPA [39] on a set of 5 uncorrelated replicas over 10 different time steps. Inset displays examples of deadlocks found at $n_{\mathrm{LEF}} = 2$. (f) Average mean squared displacement (MSD) of the center of mass (COM) of polymers with its relative standard deviation. Inset displays the diffusion coefficient of the COM of polymers normalized to the unextruded system as a function of n_{LEF}.

intriguing that deadlocks had been found previously in systems of ring polymers out of equilibrium [48,49]; it would thus be intriguing to understand if these deadlocks are also caused by the activity of the loop extruders. Moreover, in both Figs. 2(d) and 2(e), solutions with $n_{\mathrm{LEF}} = 200$ appear to undergo mild re-entanglement, arguably due to the backbone stiffening we previously observed. These findings are in line with experiments on synthetic bottlebrush polymers [43,50,51] which display greatly weakened entanglements with respect to their linear counterpart.

B. Loop extrusion speeds up polymer dynamics

Having quantified the dramatic change in the static properties of the solution, we expect to observe a similar large impact of loop extrusion on polymer dynamics. In Fig. 2(f), we show that the MSD of the COM of polymers displays a significant speed up compared with the NE case. More specifically, the diffusion coefficient of the COM of polymers, computed as $D = \lim_{t\to\infty} \mathrm{MSD}/6t$ in the system with $N/n_{\mathrm{LEF}} = 20$, is roughly 5 times larger than the control. Thus, while our results confirm the hypothesis that purely intrachain loop extrusion leads to an effective fluidification (or entanglement dilution) due to the transition from linear to bottlebrushlike structures [21,26], they also suggest that too many LEFs would drive re-entanglement in dense solutions due to backbone stiffening. However, this re-entanglement does not affect the increase in diffusivity, a result that could be due to a lower degree of interpenetration between side chains and thus reduced friction [52].

C. Loop-extrusion-mediated fluidification is length dependent

We argue that this speed up in dynamics, or fluidification, ought to be even more dramatic in more entangled systems, for instance, in denser systems or for longer chains. To test this, we performed simulations with shorter ($N = 250$ and 500) and longer ($N = 1500$) chains at fixed volume fraction ($\phi = 0.05$) and fixed LEF densities ($N/n_{\mathrm{LEF}} = 10$), as reported in Fig. 3. First, we discover that loop extrusion compacts all polymer lengths down to similar sizes and that the steady state $\langle R_g^2 \rangle$ scales roughly linearly with n_{LEF} [Fig. 3(a)], which is consistent with the expected scaling [23] $R_g^2 \sim L_{bb} L_{sl}^{1/2}$, where L_{bb} is the length of the backbone

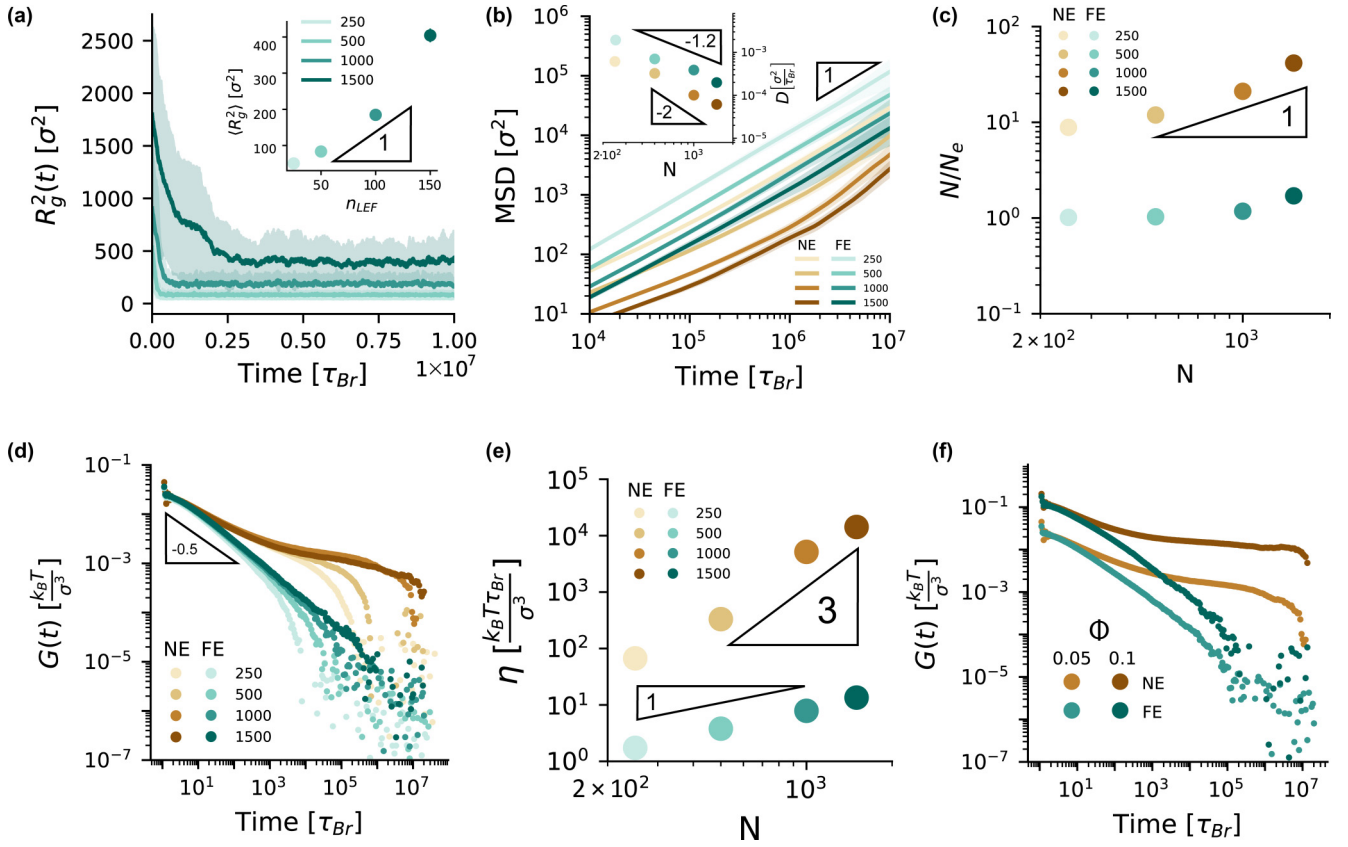

FIG. 3. (a) Average radius of gyration of polymers during extrusion and after equilibration for three different values of N. The faded area represents the width of the area covered by the distribution within the standard deviation. Inset shows the equilibrium value against n_{LEF}. (b) Average mean squared displacement (MSD) of the center of mass (COM) of polymers with its relative standard deviation for nonextruded (NE) and fully extruded (FE) systems. Inset shows the diffusion coefficient of the COM of polymers against the polymer length. (c) Number of entanglements for FE and NE configurations with different polymer length (from 250 to 1500 beads) and same loop extruding factor (LEF) density ($n_{\mathrm{LEF}} = 100$). (d) Stress-relaxation function $G(t)$ of NE and FE solutions in equilibrium. (e) Viscosity of extruded and NE systems obtained by integration of the stress-relaxation function. (f) Stress-correlation function of two 1000-bead-long polymer systems with different volume fraction (0.05 and 0.1). Values in green represent FE systems with $n_{\mathrm{LEF}} = 100$, while brown values correspond to NE systems.

(determined by the number of extruders) and L_{sl} the length of side loops (determined by N/n_{LEF}).

By comparing the dynamics of the COM MSD, we observe that, in all extruded solutions, there is a clear loss of the early-time subdiffusive regime [Fig. 3(b)] as previously observed in solutions of bottlebrush polymers [53]. For NE configurations, the diffusion coefficient of the COM scales close to the expected $D \sim N^{-2}$ [54]. On the other hand, for extruded solutions, we find $D \sim N^{-1.2}$. Interestingly, at our optimal disentanglement density (1 LEF every 10 beads), we achieve total disentanglement for every tested configuration. This reflects on average the number of entanglements per polymer, displayed in Fig. 3(c). In entangled conditions, this scales almost linearly with N, i.e., with the length of the linear chain, while after extrusion, it is constant and ∼5, displaying a similar level of entanglement independent of the polymer length.

To quantify the change in viscoelasticity due to the extrusion, we use the GK relation and compute the autocorrelation of the off-diagonal components of the stress tensor $G(t)$ [41]. From these measurements, we estimate a value of entanglement plateau of $(1.6 \pm 0.1) \times 10^{-3} k_B T/\sigma^3$, from which, combining Eqs. (5) and (6) in Ref. [44], we obtain an effective entanglement length of $27 \pm 3\sigma$, closer to the theoretical estimate $N_e = 43\sigma$. The familiar entanglement plateau observed for linear polymers [31] is completely lost in all extruded solutions, which instead follow a decay $G(t) \sim t^{-1/2}$, as for unentangled chains [Fig. 3(d)]. We interpret this as a strong signature that most of the entanglements are lost, even for our longest polymers $N = 1500$ which display $N/N_e \simeq 17$ in equilibrium. Perhaps more remarkably, the viscosity $\eta = \int_0^\infty G(t)dt$, typically scaling as $\eta \sim N^3$ for linear polymers, scales only linearly ($\eta \sim N$) in the FE cases [Fig. 3(e)]. The weak scaling of viscosity as a function of the polymerization index is in line with previous experimental results on densely grafted bottlebrushes [51].

These findings strongly suggest that the fluidification mechanism is more dramatic in solutions of longer polymers as $\eta_{\mathrm{LEF}}/\eta_0 \sim N^{-2}$. For example, for our $N = 1500$ system, the viscosity of the extruded system is ∼1000 times smaller than the NE one. Furthermore, we find even stronger fluidification in denser systems. To infer how the system density affects the extrusion-mediated viscosity reduction, we proceeded to simulate a system of 50 polymers with $N = 1000$ and volume fraction 0.1. The stress-correlation functions

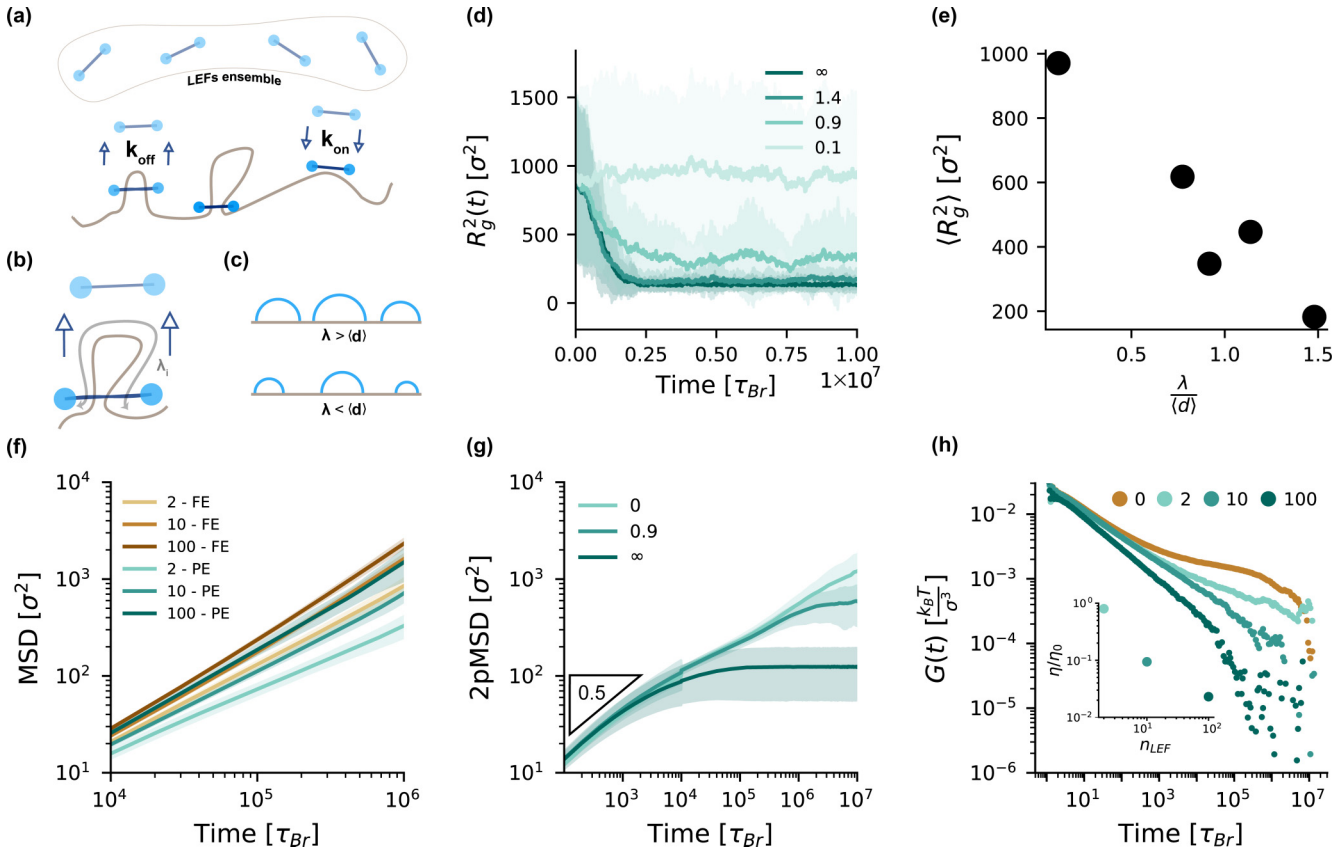

FIG. 4. (a) Sketch of our transient extrusion algorithm. Loop extruding factor (LEF) performs extrusion until they are removed with probability k_{off}, while nonbinded LEFs can start extruding with probability k_{on}. (b) Sketch of how the extruded length for a structural maintenance of chromosomes (SMC; λ_i) is estimated. (c) Sketch of extruded systems depending on the average processivity. (d) Average radius of gyration of polymers during extrusion and after equilibration for different values of $\lambda/\langle d\rangle$. In this context, $\lambda/\langle d\rangle = \infty$ means that the polymer is fully extruded (FE), and $\lambda/\langle d\rangle = 0$ means that the polymer is nonextruded (NE). (e) Radius of gyration squared against normalized processivity. We multiply processivity by the number of LEFs per polymer and divide for the polymer length to get a collapse plot. (f) Average mean squared displacement (MSD) for the center of mass of FE and partially extruded (PE) polymers with $\lambda/\langle d\rangle \simeq 1$ and different numbers of LEFs (2–100). (g) Two-point MSD taken as the average distance between two beads belonging to the same polymer with a contour distance of 600 beads with different values of $\lambda/\langle d\rangle$. (f) Stress-relaxation modulus of NE and PE systems with $\lambda/\langle d\rangle \simeq 1$ and different numbers of n_{LEF}. Inset shows the relative viscosity normalized to the viscosity of the NE system.

displayed in Fig. 3(f) display identical properties between the two systems. However, the viscosity computed from such function shows a ≈2000-fold reduction in viscosity between the NE and extruded configuration, showing a consistent increment from the ≈1000-fold decrease obtained for the less dense system. By extrapolating these results to genomic-sized DNA, we expect the difference between the dynamics of chromosomes in the presence/absence of (purely intrachain and nonbridging) LEFs will be several orders of magnitude. This implies that the large-scale rearrangement and dynamics of interphase and mitotic chromosomes are expected to be sensitive to the presence of active loop extrusion and may be tested in experiments via, e.g., displacement correlation spectroscopy [18,28,55–57].

D. Out-of-equilibrium entangled solutions of transiently loop extruding polymers

Having quantified the fluidification achieved in a FE steady state, we now turn our attention to the behavior of our system under an out-of-equilibrium, active-loop extrusion process for $N = 1000$. The total number of LEFs in the simulation is fixed, but the number bound at any one time fluctuates around the mean fraction $f_{\text{bound}} = \kappa_{\text{on}}/(\kappa_{\text{on}} + \kappa_{\text{off}})$. In the following, we focus on the so-called partially extruded (PE) case, in which the total extruded length is smaller than N, i.e., the LEFs kinetically unbind from the polymer before they can fully extrude the average distance between them [see Fig. 4(a)]. We highlight that the regime of PE is the one that appears to be most relevant in interphase [18,58] and is characterized by the ratio between the average processivity and the average spacing between LEFs, i.e., $\lambda/\langle d\rangle = \langle v_{\text{LEF}}\rangle/\kappa_{\text{off}} \times N/n_{\text{LEF}}$ [see Fig. 4(b)]. For instance, in PE solutions, $\lambda/\langle d\rangle < 1$.

First, we find that the radius of gyration of the polymers depends on $\lambda/\langle d\rangle$: Small values yield NE polymers, while larger values yield a compaction like the FE case (where $\lambda/\langle d\rangle \to \infty$ as $k_{\text{off}} = 0$). Interestingly, we also observe stable, intermediate compacted states in between a FE and NE state where the polymer is kept out of equilibrium by the kinetic binding of LEFs [Fig. 4(d)].

In Fig. 4(e), we display the distribution of the squared radius of gyration and connect its value to the average processivity of extruders. When the normalized processivity is very high (>1), we get systems with radius of gyration like the FE ones. When the normalized processivity is small (<1), we instead get systems with radius of gyration close to the NE case. For intermediate values, we find steady states with similar radii of gyration independently on the total number of SMCs in the system.

Despite being only PE, the average MSD for the COM of the polymers [Fig. 4(f)] shows the loss of elastic behavior at early times while also displaying the LEF-dependent increase in diffusivity. However, the value of PE-related MSDs is found to always be smaller than the correspondent FE MSDs.

To make a comparison with experiments, we compute the 2-point MSD [18,55], i.e., the autocorrelation of the distance vector $\mathbf{d}$ between two given polymer segments separated by the curvilinear distance l or $2\text{pMSD}(t, l) = \langle[\mathbf{d}(t_0 + t, s + l) - \mathbf{d}(t_0, s)]^2\rangle_{t_0,s}$. In line with recent experiments [18,55,56] and Rouse theory, we observe a short-time scaling $2\text{pMSD}(t) \sim t^{1/2}$ that is surprisingly unaffected by the loop extrusion [Fig. 4(g)]. A quantitatively different behavior of the $2\text{pMSD}(t)$ is seen only at large times due to the different polymer compaction, in agreement with experiments implementing rapid cohesin knockouts [18,58]. At intermediate time scales, both the NE and PE cases display $2\text{pMSD}(t) \sim t^{1/3}$, which is consistent with the one observed in experiments with embryo cells [55].

Finally, we also compute the stress-relaxation function $G(t)$ for this out-of-equilibrium PE scenario, and once again, we observe a clear lack of entanglement plateaus in the presence of LEFs [Fig. 4(h)]. In turn, this translates into a significantly smaller effective viscosity of the PE solution, which depends on the dimensionless ratio $\lambda/\langle d\rangle$. For PE solutions ($\lambda/\langle d\rangle \simeq 1$), the viscosity is 100-fold smaller than the control, and we expect the same scaling with polymer length seen in Fig. 3. Importantly, we find that stopping the loop extrusion process and performing GK calculation yields the same $G(t)$ as the one obtained while loop extrusion is ongoing (not shown). This confirms that the loop extrusion *per se* does not affect the viscoelasticity of the solution, but rather it does so indirectly through the change in polymer conformation.

IV. CONCLUSIONS

Motivated by the lack of understanding of how loop extrusion affects polymer entanglement and dynamics in dense solutions, we performed large-scale molecular dynamics simulations of entangled polymers under the action of LEFs. The first main discovery of our work is that loop extrusion, when it is exclusively intrachain, dramatically decreases the entanglement between chains in dense solutions. This result supports previous works suggesting that loop extrusion drives entanglement dilution [21,26]; we provide a solid numerical quantification of this effect through the use of PPA in dense solutions. FE chains display no sign of entanglement, and in fact, they self-organize into territories (Figs. 1 and 2). We then discovered that the mobility of the polymers is strongly sped up by the extrusion process, in turn yielding an effective fluidification of the solutions, leading to a much weaker scaling of viscosity $\eta \sim L$ (in contrast with $\eta \sim L^3$ for entangled systems) and a reduction up to 1000-fold for our longest polymers (Fig. 3). These effects are in line with the fact that synthetic bottlebrush polymers are more weakly entangled than their linear counterparts [43]. Finally, we considered the case of PE using a transient binding model and showed that, even in the PE situation, with kinetic binding/unbinding of LEFs, the viscosity of polymer solutions is greatly reduced via the active extrusion process (Fig. 4).

Our findings suggest that loop extrusion may have a marked effect on the large-scale organization and viscoelasticity of the nucleoplasm, through the change in conformation and dynamics of chromosomes. We note that our results are strongly dependent on the fact that we assumed loop extrusion to be exclusively intrachain since we have neglected the formation of Z loops for computational simplicity. We argue that, despite being observed in bacteria [59] and *in vitro* [60], there is no evidence of Z loops formed in eukaryotes. We expect that considering interchain loop extrusion [36,61] and bridging [37] may drastically influence our results, eventually decreasing the mobility of the polymers and thus increasing the viscoelasticity of the solution. It will be interesting to test this scenario in the future.

ACKNOWLEDGMENTS

D.M. acknowledges the Royal Society and the European Research Council (Grant Agreement No. 947918, TAP) for funding. The authors also acknowledge the contribution of the COST Action Eutopia, Grant No. CA17139. For the purpose of open access, the author has applied a Creative Commons Attribution (CC BY) licence to any author accepted manuscript version arising from this submission.

[1] E. Lieberman-Aiden, N. L. van Berkum, L. Williams, M. Imakaev, T. Ragoczy, A. Telling, I. Amit, B. R. Lajoie, P. J. Sabo, M. O. Dorschner *et al.*, Comprehensive mapping of long-range interactions reveals folding principles of the human genome, Science **326**, 289 (2009).

[2] R. A. Beagrie, A. Scialdone, M. Schueler, D. C. A. Kraemer, M. Chotalia, S. Q. Xie, M. Barbieri, I. de Santiago, L.-M. Lavitas, M. R. Branco *et al.*, Complex multi-enhancer contacts captured by genome architecture mapping, Nature (London) **543**, 519 (2017).

[3] T. Cremer and C. Cremer, Chromosome territories, nuclear architecture and gene regulation in mammalian cells, Nat. Rev. Genet. **2**, 292 (2001).

[4] C. Brackley, M. Pereira, J. Johnson, D. Michieletto, and D. Marenduzzo, Predictive models for 3D chromosome organization: The transcription factor and diffusive loop extrusion

models, *in Modeling the 3D Conformation of Genomes*, edited by G. Tiana and L. Giorgetti (CRC Press, Boca Raton, 2019).

[5] J. Dekker, M. A. Marti-Renom, and L. A. Mirny, Exploring the three-dimensional organization of genomes: Interpreting chromatin interaction data, Nat. Rev. Genet. **14**, 390 (2013).

[6] J. Nuebler, G. Fudenberg, M. Imakaev, N. Abdennur, and L. A. Mirny, Chromatin organization by an interplay of loop extrusion and compartmental segregation, Proc. Nat. Acad. Sci. USA **115**, E6697 (2018).

[7] K. Nasmyth, Cohesin: A catenase with separate entry and exit gates? Nat. Cell Biol. **13**, 1170 (2011).

[8] E. Alipour and J. F. Marko, Self-organization of domain structures by DNA-loop-extruding enzymes, Nucl. Acids Res. **40**, 11202 (2012).

[9] G. Fudenberg, M. Imakaev, C. Lu, A. Goloborodko, N. Abdennur, and L. A. Mirny, Formation of chromosomal domains by loop extrusion, Cell Rep. **15**, 2038 (2016).

[10] A. L. Sanborn, S. S. P. Rao, S.-C. Huang, N. C. Durand, M. H. Huntley, A. I. Jewett, I. D. Bochkov, D. Chinnappan, A. Cutkosky, J. Li *et al.*, Chromatin extrusion explains key features of loop and domain formation in wild-type and engineered genomes, Proc. Natl. Acad. Sci. USA **112**, E6456 (2015).

[11] I. F. Davidson, B. Bauer, D. Goetz, W. Tang, G. Wutz, and J.-M. Peters, DNA loop extrusion by human cohesin, Science **366**, 1338 (2019).

[12] M. Ganji, I. A. Shaltiel, S. Bisht, E. Kim, A. Kalichava, C. H. Haering, and C. Dekker, Real-time imaging of DNA loop extrusion by condensin, Science **360**, 102 (2018).

[13] B. Pradhan, T. Kanno, M. U. Igarashi, M. S. Loke, M. D. Baaske, J. S. K. Wong, K. Jeppsson, C. Björkegren, and E. Kim, The Smc5/6 complex is a DNA loop-extruding motor, Nature (London) **616**, 843 (2023).

[14] A. S. Câmara, V. Schubert, M. Mascher, and A. Houben, A simple model explains the cell cycle-dependent assembly of centromeric nucleosomes in holocentric species, Nucl. Acids Res. **49**, 9053 (2021).

[15] L. Vian, A. Pękowska, S. S. Rao, K. R. Kieffer-Kwon, S. Jung, L. Baranello, S. C. Huang, L. El Khattabi, M. Dose, N. Pruett *et al.*, The energetics and physiological impact of cohesin extrusion, Cell **173**, 1165 (2018).

[16] J. H. Gibcus, K. Samejima, A. Goloborodko, I. Samejima, N. Naumova, J. Nuebler, M. T. Kanemaki, L. Xie, J. R. Paulson, W. C. Earnshaw *et al.*, A pathway for mitotic chromosome formation, Science **359**, eaao6135 (2018).

[17] M. Conte, E. Irani, A. M. Chiariello, A. Abraham, S. Bianco, A. Esposito, and M. Nicodemi, Loop-extrusion and polymer phase-separation can co-exist at the single-molecule level to shape chromatin folding, Nat. Commun. **13**, 4070 (2022).

[18] M. Gabriele, H. B. Brandão, S. Grosse-Holz, A. Jha, G. M. Dailey, C. Cattoglio, T.-H. S. Hsieh, L. Mirny, C. Zechner, and A. S. Hansen, Dynamics of CTCF- and cohesin-mediated chromatin looping revealed by live-cell imaging, Science **376**, 496 (2022).

[19] A. Goloborodko, J. F. Marko, and L. A. Mirny, Chromosome compaction by active loop extrusion, Biophys. J. **110**, 2162 (2016).

[20] E. J. Banigan and L. A. Mirny, Limits of chromosome compaction by loop-extruding motors, Phys. Rev. X **9**, 031007 (2019).

[21] K. E. Polovnikov, H. B. Brandão, S. Belan, B. Slavov, M. Imakaev, and L. A. Mirny, Crumpled polymer with loops recapitulates key features of chromosome organization, Phys. Rev. X **13**, 041029 (2023).

[22] J. F. Marko and E. D. Siggia, Polymer models of meiotic and mitotic chromosomes, Mol. Biol. Cell **8**, 2217 (1997).

[23] J. Paturej, S. S. Sheiko, S. Panyukov, and M. Rubinstein, Molecular structure of bottlebrush polymers in melts, Sci. Adv. **2**, e1601478 (2016).

[24] D. Racko, F. Benedetti, D. Goundaroulis, and A. Stasiak, Chromatin loop extrusion and chromatin unknotting, Polymers **10**, 1126 (2018).

[25] E. Orlandini, D. Marenduzzo, and D. Michieletto, Synergy of topoisomerase and structural-maintenance-of-chromosomes proteins creates a universal pathway to simplify genome topology, Proc. Natl. Acad. Sci. USA **116**, 8149 (2019).

[26] B. Chan and M. Rubinstein, Activity-driven chromatin organization during interphase: Compaction, segregation, and entanglement suppression, Proc. Natl. Acad. Sci. USA **121**, e2401494121 (2024).

[27] J. Paturej and A. Erbaş, Cyclic-polymer grafted colloids in spherical confinement: Insights for interphase chromosome organization, Phys. Biol. **20**, 056004 (2023).

[28] A. Zidovska, D. A. Weitz, and T. J. Mitchison, Micron-scale coherence in interphase chromatin dynamics, Proc. Nat. Acad. Sci. USA **110**, 15555 (2013).

[29] D. Saintillan, M. J. Shelley, and A. Zidovska, Extensile motor activity drives coherent motions in a model of interphase chromatin, Proc. Nat. Acad. Sci. USA **115**, 11442 (2018).

[30] C. M. Caragine, S. C. Haley, and A. Zidovska, Surface fluctuations and coalescence of nucleolar droplets in the human cell nucleus, Phys. Rev. Lett. **121**, 148101 (2018).

[31] K. Kremer and G. S. Grest, Dynamics of entangled linear polymer melts: A molecular-dynamics simulation, J. Chem. Phys. **92**, 5057 (1990).

[32] L. Tubiana, G. P. Alexander, A. Barbensi, D. Buck, J. H. Cartwright, M. Chwastyk, M. Cieplak, I. Coluzza, S. Čopar, D. J. Craik *et al.*, Topology in soft and biological matter, Phys. Rep. **1075**, 1 (2024).

[33] S. Plimpton, Fast parallel algorithms for short-range molecular dynamics, J. Comput. Phys. **117**, 1 (1995).

[34] See Supplemental Material at http://link.aps.org/supplemental/10.1103/PhysRevResearch.6.033160 for a movie showing how loop extrusion changes the shape of the entangled polymers in the simulated solution.

[35] https://git.ecdf.ed.ac.uk/taplab/smc-lammps

[36] A. Bonato and D. Michieletto, Three-dimensional loop extrusion, Biophys. J. **120**, 5544 (2021).

[37] J.-K. Ryu, C. Bouchoux, H. W. Liu, E. Kim, M. Minamino, R. de Groot, A. J. Katan, A. Bonato, D. Marenduzzo, D. Michieletto *et al.*, Bridging-induced phase separation induced by cohesin SMC protein complexes, Sci. Adv. **7**, eabe5905 (2021).

[38] J. D. Halverson, W. B. Lee, G. S. Grest, A. Y. Grosberg, and K. Kremer, Molecular dynamics simulation study of nonconcatenated ring polymers in a melt. I. Statics, J. Chem. Phys. **134**, 204904 (2011).

[39] R. Everaers, S. K. Sukumaran, G. S. Grest, C. Svaneborg, A. Sivasubramanian, and K. Kremer, Rheology and microscopic

topology of entangled polymeric liquids, Science **303**, 823 (2004).

[40] W. B. Lee and K. Kremer, Entangled polymer melts: Relation between plateau modulus and stress autocorrelation function, Macromolecules **42**, 6270 (2009).

[41] J. Ramírez, S. K. Sukumaran, B. Vorselaars, and A. E. Likhtman, Efficient on the fly calculation of time correlation functions in computer simulations, J. Chem. Phys. **133**, 154103 (2010).

[42] H.-M. Chun, Q. Gao, and J. M. Horowitz, Nonequilibrium Green-Kubo relations for hydrodynamic transport from an equilibrium-like fluctuation-response equality, Phys. Rev. Res. **3**, 043172 (2021).

[43] W. F. Daniel, J. Burdyńska, M. Vatankhah-Varnoosfaderani, K. Matyjaszewski, J. Paturej, M. Rubinstein, A. V. Dobrynin, and S. S. Sheiko, Solvent-free, supersoft and superelastic bottlebrush melts and networks, Nat. Mater. **15**, 183 (2016).

[44] N. Uchida, G. S. Grest, and R. Everaers, Viscoelasticity and primitive path analysis of entangled polymer liquids: From F-actin to polyethylene, J. Chem. Phys. **128**, 044902 (2008).

[45] H. Liang, G. S. Grest, and A. V. Dobrynin, Brush-like polymers and entanglements: From linear chains to filaments, ACS Macro Lett. **8**, 1328 (2019).

[46] H. Xiong, T. Yue, Q. Wu, L. Zhang, Z. Xie, J. Liu, L. Zhang, and J. Wu, Self-healing bottlebrush polymer networks enabled via a side-chain interlocking design, Mater. Horiz. **10**, 2128 (2023).

[47] D. Michieletto and M. S. Turner, A topologically driven glass in ring polymers, Proc. Natl. Acad. Sci. USA **113**, 5195 (2016).

[48] C. Micheletti, I. Chubak, E. Orlandini, and J. Smrek, Topology-based detection and tracking of deadlocks reveal aging of active ring melts, ACS Macro Lett. **13**, 124 (2024).

[49] T. C. O'Connor, T. Ge, M. Rubinstein, and G. S. Grest, Topological linking drives anomalous thickening of ring polymers in weak extensional flows, Phys. Rev. Lett. **124**, 027801 (2020).

[50] L. H. Cai, T. E. Kodger, R. E. Guerra, A. F. Pegoraro, M. Rubinstein, and D. A. Weitz, Soft poly(dimethylsiloxane) elastomers from architecture-driven entanglement free design, Adv. Mater. **27**, 5132 (2015).

[51] M. Hu, Y. Xia, G. B. McKenna, J. A. Kornfield, and R. H. Grubbs, Linear rheological response of a series of densely branched brush polymers, Macromolecules **44**, 6935 (2011).

[52] M. Abbasi, L. Faust, and M. Wilhelm, Comb and bottlebrush polymers with superior rheological and mechanical properties, Adv. Mater. **31**, 1806484 (2019).

[53] M. Abbasi, L. Faust, K. Riazi, and M. Wilhelm, Linear and extensional rheology of model branched polystyrenes: From loosely grafted combs to bottlebrushes, Macromolecules **50**, 5964 (2017).

[54] M. Doi and S. Edwards, *The Theory of Polymer Dynamics* (Oxford University Press, Oxford, 1988).

[55] A. K. Yesbolatova, R. Arai, T. Sakaue, and A. Kimura, Formulation of chromatin mobility as a function of nuclear size during *C. elegans* embryogenesis using polymer physics theories, Phys. Rev. Lett. **128**, 178101 (2022).

[56] D. B. Brückner, H. Chen, L. Barinov, B. Zoller, and T. Gregor, Stochastic motion and transcriptional dynamics of pairs of distal DNA loci on a compacted chromosome, Science **380**, 1357 (2023).

[57] H. A. Shaban, R. Barth, and K. Bystricky, Formation of correlated chromatin domains at nanoscale dynamic resolution during transcription, Nucl. Acids Res. **46**, e77 (2018).

[58] D. Michieletto and W. A. Bickmore, TADs do not stay in the loop, Mol. Cell **82**, 2188 (2022).

[59] H. B. Brandão, Z. Ren, X. Karaboja, L. A. Mirny, and X. Wang, DNA-loop-extruding SMC complexes can traverse one another in vivo, Nat. Struct. Mol. Biol. **28**, 642 (2021).

[60] E. Kim, J. Kerssemakers, I. A. Shaltiel, C. H. Haering, and C. Dekker, DNA-loop extruding condensin complexes can traverse one another, Nature (London) **579**, 438 (2020).

[61] J.-K. Ryu, S.-H. Rah, R. Janissen, J. W. J. Kerssemakers, A. Bonato, D. Michieletto, and C. Dekker, Condensin extrudes DNA loops in steps up to hundreds of base pairs that are generated by ATP binding events, Nucl. Acids Res. **50**, 820 (2022).